Supplementary Material: On how monospecific memory-like autoregulatory CD8$^+$ T cells can blunt diabetogenic autoimmunity: a computational approach

Anmar Khadra[a,*], Sue Tsai[b], Pere Santamaria[b] and Leah Edelstein-Keshet[c]

[a]Laboratory of Biological Modeling, National Institutes of Health, Bethesda, Md 20892-5621 USA

[b]Julia McFarlane Diabetes Research Centre, Department of Microbiology and Infectious Diseases Faculty of Medicine, University Calgary, Calgary, AB, T2N 4N1 Canada

[c]Department of Mathematics and Institute of Applied Mathematics University of British Columbia, Vancouver, BC, Z6T 1Z2 Canada

September 7, 2010

Downloaded from http://journals.aai.org/jimmunol/article-supplement/82846/pdf/jimmunol1001306-sup-suppdata/ by guest on 06 August 2024

1 Basic model

The full basic model for T cell dynamics (before treatment) consists of the following equations.

$$\frac{dM}{dt} = (\overline{\sigma}_m + \overline{\alpha}_m M)A\overline{f}_m(P_1) - \delta_m M - \frac{\overline{\epsilon}}{A}M(M+E+Z), \tag{1a}$$

$$\frac{dE}{dt} = (\overline{\sigma}_e + \overline{\alpha}_e E)A\overline{f}_e(P_1) - \delta_e E - \frac{\overline{\epsilon}}{A}E(M+E+Z), \tag{1b}$$

$$\frac{dZ}{dt} = (\overline{\sigma}_z + \overline{\alpha}_z Z)A\overline{f}_z(P_2) - \delta_z Z - \frac{\overline{\epsilon}}{A}Z(M+E+Z), \tag{1c}$$

$$\frac{dB}{dt} = s\frac{B}{k_B+B} - \delta_B B + \frac{\kappa(E+\phi Z)B}{1+\mu_0 B+\mu_1 M}, \tag{1d}$$

$$\frac{dP_1}{dt} = \overline{R}_1\frac{(E+\phi Z)B}{1+\mu B} - \delta_{p_1}P_1, \tag{1e}$$

$$\frac{dP_2}{dt} = \overline{R}_2\frac{(E+\phi Z)B}{1+\mu B} - \delta_{p_2}P_2, \tag{1f}$$

$$\frac{dA}{dt} = \sigma_a - k_a MA - \delta_a A, \tag{1g}$$

$$\overline{f}_i(P_1) \equiv \frac{P_1^2}{K_i^2+P_1^2} \quad (i=m,e), \tag{1h}$$

$$\overline{f}_z(P_2) \equiv \frac{P_2^2}{K_z^2+P_2^2}. \tag{1i}$$

Parameters are as defined in Table 1 in the paper.

2 Reduced model for competition of three T cell pools

We assume here that β cells and APCs are both at constant population levels (B, A=constant). By applying quasi-steady state (QSS) assumption on autoantigen peptide ($dP_j/dt \approx 0, j = 1, 2$), we obtain $P_j \approx R_j(E + \phi Z)$, where we have defined

$$R_j = \frac{\overline{R}_j}{\delta_{p_j}} C_B = \frac{\overline{R}_j}{\delta_{p_j}} \left(\frac{B}{(1 + \mu B)} \right), \quad j = 1, 2,$$

The term in braces, is assumed to be constant (=C_B) in this paper. Then

$$\tilde{f}_i(E + \phi Z) \equiv \frac{(E + \phi Z)^2}{k_i^2 + (E + \phi Z)^2}, \quad i = m, e, z,$$

where $k_i = K_i/R_1$, $i = m, e$, and $k_z = K_z/R_2$.

Thus the reduced model consists of three populations of T cells, memory (M), dominant effector (E) and subdominant effector (Z) CD8$^+$ T cells:

$$\frac{dM}{dt} = (\sigma_m + \alpha_m M)\tilde{f}_m(E + \phi Z) - \delta_m M - \epsilon M(M + E + Z), \tag{2a}$$

$$\frac{dE}{dt} = (\sigma_e + \alpha_e E)\tilde{f}_e(E + \phi Z) - \delta_e E - \epsilon E(M + E + Z), \tag{2b}$$

$$\frac{dZ}{dt} = (\sigma_z + \alpha_z Z)\tilde{f}_z(E + \phi Z) - \delta_z Z - \epsilon Z(M + E + Z), \tag{2c}$$

where $\alpha_i = \overline{\alpha_i} A \approx \overline{\alpha_i} A_d$, for $i = m, e, z$, and $\epsilon = \overline{\epsilon}/A \approx \overline{\epsilon}/A_d$ (A_d is the number of APCs during the autoimmune attack). Here the parameters δ_z, α_z and k_z represent the average values of such parameters over all clones included in this population, while $\phi \leq 1$. Moreover, as described in the text,

$$\delta_e > \delta_z > \delta_m, \quad \alpha_m > \alpha_z \geq \alpha_e, \quad k_m > k_z > k_e, \quad \sigma_m \approx \sigma_e \approx \sigma_z. \tag{3}$$

Thymic input of naive T cells has a very small effect on the general dynamics of the model relative to T cell expansion rates (see below). It will therefore be neglected from our analysis unless otherwise stated.

2.1 Geometrical analysis

We aim in this section to establish that when $\sigma_i = 0$, $i = m, e, z$, any isolated equilibrium point of system (2a)-(2c) must have at least one zero component, i.e. that one or more of the T cell pools go extinct. In order to do so, we first observe that the coordinate planes $M = 0$, $E = 0$ and $Z = 0$ are nullsurfaces, and so are the surfaces described

Downloaded from http://journals.aai.org/jimmunol/article-supplement/82846/pdf/jimmunol1001306-sup-suppdata/ by guest on 06 August 2024

by the equations

$$\alpha_m \tilde{f}_m(E+\phi Z) - \delta_m = \epsilon(M+E+Z), \tag{4a}$$

$$\alpha_e \tilde{f}_e(E+\phi Z) - \delta_e = \epsilon(M+E+Z), \tag{4b}$$

$$\alpha_z \tilde{f}_z(E+\phi Z) - \delta_z = \epsilon(M+E+Z). \tag{4c}$$

(These are M, E and Z nullsurfaces, respectively). We now show that the intersection of any two nullsurfaces given by Eqs. (4a)-(4c) is a line parallel to the EZ-plane. From Eqs. (4a) and (4b) (the M and E nullsurfaces), we can conclude that

$$\alpha_m \tilde{f}_m(E+\phi Z) - \delta_m = \alpha_e \tilde{f}_e(E+\phi Z) - \delta_e. \tag{5}$$

By letting $Y = E + \phi Z$ and substituting the expressions for $\tilde{f}_m$ and $\tilde{f}_e$ into (5), we obtain

$$A_1 Y^4 + B_1 Y^2 + C_1 = 0,$$

where $A_1 := \alpha_m - \alpha_e - \delta_1$, $B_1 := (\alpha_m - \delta_1)k_e^2 - (\alpha_e + \delta_1)k_m^2$ and $C_1 := -\delta_1 k_m^2 k_e^2$ (with $\delta_1 = \delta_m - \delta_e$). It follows that the intersection of the two nullsurfaces is given by $E + \phi Z = \pm\mathcal{L}_1$, where

$$\mathcal{L}_1 \equiv \frac{-B_1 \pm \sqrt{B_1^2 - 4A_1C_1}}{2A_1} \geq 0.$$

For equilibrium points lying inside or on the boundary of the first octant, we choose the two lines $E + \phi Z = \mathcal{L}_1$ to represent the intersections of the M and E nullsurfaces. While these two lines are parallel to the EZ-plane and never intersect it, they intersect the nullsurfaces $E = 0$ and $Z = 0$. By applying the same technique, we may also show that the M and Z nullsurfaces expressed by Eqs. (4a) and (4c) intersect at the two lines $E + \phi Z = \mathcal{L}_2$, while the E and Z nullsurfaces expressed by Eqs. (4b) and (4c) intersect at the two lines $E + \phi Z = \mathcal{L}_3$, where

$$\mathcal{L}_2 \equiv \frac{-B_2 \pm \sqrt{B_2^2 - 4A_2C_2}}{2A_2} \geq 0$$

and

$$\mathcal{L}_3 \equiv \frac{-B_3 \pm \sqrt{B_3^2 - 4A_3C_3}}{2A_3} \geq 0.$$

Here $A_2 := \alpha_m - \alpha_z - \delta_2$, $B_2 := (\alpha_m - \delta_2)k_z^2 - (\alpha_z + \delta_2)k_m^2$, $C_2 := -\delta_2 k_m^2 k_z^2$, $A_3 := \alpha_e - \alpha_z - \delta_3$, $B_3 := (\alpha_e - \delta_3)k_z^2 - (\alpha_z + \delta_3)k_e^2$ and $C_3 := -\delta_3 k_e^2 k_z^2$ (with $\delta_2 = \delta_m - \delta_z$ and $\delta_3 = \delta_e - \delta_z$). Clearly, these lines never intersect each other unless $\mathcal{L}_{j_1} = \mathcal{L}_{j_2}$ ($j_1, j_2 = 1, 2, 3$), when they actually coincide and generate a line of nonisolated and unstable equilibria. In other words, system (2a)-(2c) cannot possess isolated equilibrium points lying inside the first octant. The only steady states this system may possess are those that lie on the coordinate planes with at least one zero component.

Downloaded from http://journals.aai.org/jimmunol/article-supplement/82846/pdf/jimmunol1001306-sup-suppdata/ by guest on 06 August 2024

It should be mentioned here that the same conclusion can be reached for arbitrary functions $\tilde{f}_i$, $i = m, e, z$. The proof of this result is similar to the one shown above.

2.2 Scaling the variables

By scaling the variables M, E and Z using the substitutions

$$m = \frac{M}{k_e}, \quad e = \frac{E}{k_e}, \quad z = \frac{Z}{k_e},$$

we obtain

$$\frac{dm}{dt} = (\sigma_m^* + \alpha_m m) f_m(e + \phi z) - \delta_m m - \epsilon^* m(m + e + z), \tag{6a}$$

$$\frac{de}{dt} = (\sigma_e^* + \alpha_e e) f_e(e + \phi z) - \delta_e e - \epsilon^* e(m + e + z), \tag{6b}$$

$$\frac{dz}{dt} = (\sigma_z^* + \alpha_z z) f_z(e + \phi z) - \delta_z z - \epsilon^* z(m + e + z), \tag{6c}$$

where $\sigma_i^* = \sigma_i / k_e$, $i = m, e, z$, $\epsilon^* = \epsilon k_e$ and

$$f_i(e + \phi z) \equiv \frac{(e + \phi z)^2}{(k_i/k_e)^2 + (e + \phi z)^2}, \quad i = m, e, z.$$

If we assume that $\sigma_i^* \approx 0$, the nullsurfaces associated with Eqs. (6a)-(6c) become (see Fig. 1):

(a) m-nullsurfaces:

$$m = 0 \text{ and } m = \frac{\alpha_m}{\epsilon^*} f_m(e + \phi z) - \frac{\delta_m}{\epsilon^*} - (e + z) =: \widetilde{g}_m(e, z).$$

(b) e-nullsurfaces:

$$e = 0 \text{ and } m = \frac{\alpha_e}{\epsilon^*} f_e(e + \phi z) - \frac{\delta_e}{\epsilon^*} - (e + z) =: \widetilde{g}_e(e, z).$$

(c) z-nullsurfaces:

$$z = 0 \text{ and } m = \frac{\alpha_z}{\epsilon^*} f_z(e + \phi z) - \frac{\delta_z}{\epsilon^*} - (e + z) =: \widetilde{g}_z(e, z).$$

2.3 Details of the analysis

The only steady states of system (6a)-(6c) are those that lie on the coordinate planes with at least one zero component. One of these steady states is the autoimmune free (healthy state) $\mathbf{S}_1 = (0, 0, 0)$, lying at the intersection of all coordinate planes. The Jacobian matrix at that point, $J_{\mathbf{S}_1} = \text{diag}(-\delta_m, -\delta_e, -\delta_z)$, has eigenvalues $\lambda_1 = -\delta_m$, $\lambda_2 = -\delta_e$ and $\lambda_3 = -\delta_z$. Therefore, the healthy state $\mathbf{S}_1$ is always stable.

The diseased state, on the other hand, could take one of the following forms: $(0, 0, z)$, $(m, 0, z)$, $(0, e, z)$, $(m, e, 0)$ and $(0, e, 0)$, the last two of which correspond to the diseased states analyzed in (1). Stability of these states is determined by the values of the parameters appearing in the model. The presence of healthy and diabetic mice

Downloaded from http://journals.aai.org/jimmunol/article-supplement/82846/pdf/jimmunol1001306-sup-suppdata/ by guest on 06 August 2024

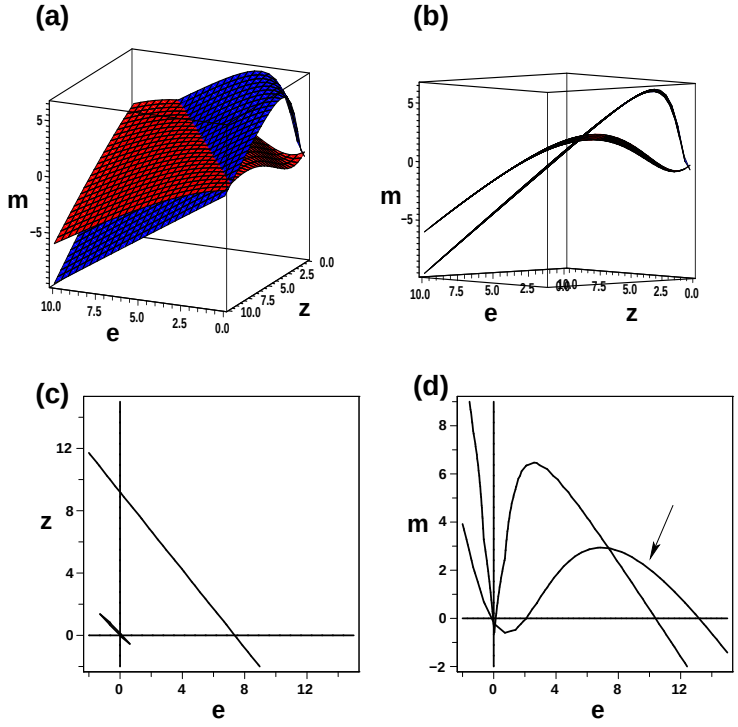

Fig. 1: The nullsurfaces $m = \widetilde{g}_m(e, z)$ (red) and $m = \widetilde{g}_e(e, z)$ (blue) of system (6a)-(6c) viewed from two different angles are shown in panels (a) and (b). The line along which these nullsurfaces intersect is projected onto the ez-plane in (c), while their intersection with the em-plane is shown in panel (d). The profiles of the nullsurfaces on the em-plane shown in panel (d) resemble the nullclines generated by the 2-variable model discussed in (1). The arrow in (d) points to the profile of $m = \widetilde{g}_m(e, z)$.

suggests that the healthy state must coexist with a stable diseased state. Some of these diseased states may even coexist but numerical evidence suggests that only one of them can be stable. Those steady states that are unstable demarcate the basin of attraction of both $\mathbf{S}_1$ and $\mathbf{S}_2$. The values of the parameter ϕ and the avidity ratio k_z/k_e play key roles in determining the structure of the diseased state. Very little is known about the values of these two parameters, but our model assumptions listed in the paper give bounds on both of them. For example, the default values listed in Table 1 generate a diseased state $\mathbf{S}_2$ that possesses only the subdominant effector T cell pool, Z, with a population size of roughly 10^6 cells. By changing the value of ϕ to 0.3, both dominant and subdominant CTL pools, E and Z, appear in the diseased state with a ratio of $3 : 2$, unlike the case when $\phi = 1$, in which memory cell pool, M, and subdominant effector cell pool, Z, appear instead with a ratio of $1 : 64$. Similarly, by reducing the value of the avidity ratio k_z/k_e to 9, the diseased state becomes free of the subdominant effector pool, Z, with a memory-to-dominant effector $(M : E)$ ratio of $1 : 20$.

Downloaded from http://journals.aai.org/jimmunol/article-supplement/82846/pdf/jimmunol1001306-sup-suppdata/ by guest on 06 August 2024

3 Treatments that expand M

To understand the effects of treatments aimed at expanding the pool of memory cells, we consider the following model in which thymic input is neglected.

$$\begin{aligned}\frac{dm}{dt} &= m(\alpha_m f_m(e+\phi z) + r_m - \delta_m - \epsilon^*(m+e+z)),\\ \frac{de}{dt} &= e(\alpha_e f_e(e+\phi z) - \delta_e - \epsilon^*(m+e+z)),\\ \frac{dz}{dt} &= z(\alpha_z f_z(e+\phi z) - \delta_z - \epsilon^*(m+e+z)),\end{aligned}$$

where r_m symbolizes such an APC-independent expansion of memory cells (here $\sigma_i^* = 0$, $i = m, e, z$). To study this model, we use bifurcation analysis, described below.

3.1 Bifurcation analysis and implications

We analyzed the bifurcation diagrams of e and z with respect to r_m within the parameter range $0 \leq r_m \leq 5$ d^{-1} (see Fig. 2, where solid lines represent stable and dashed lines represent unstable steady states).

(a) At the default values, the diseased state is of the form $(0, 0, z)$. As shown in Fig. 2(a1,2), for small increasing values of r_m, there is no effect on this state. In the range $1 \leq r_m \leq 1.5$ d^{-1}, treatments become more effective with increasing r_m; there is an observed decrease (increase) in the size of the z pool (m pool, not shown). This promising behaviour is interrupted when stability jumps from a diseased state of the form $(m_1, 0, z)$ to another one of the form $(m_2, e, 0)$, i.e. dominant effectors overcome the subdominant pool.

An increase in the parameter r_m induces an expansion in the size of the m pool in the healthy state $\mathbf{S}_1$ (results not shown). The equilibrium point $(0, 0, 0)$, on the other hand, becomes unstable (see (1) for similar behaviour). Increasing r_m shifts the curve (identified by the arrow in Fig. 1) upward, generating a new stable steady state with an elevated level of m, leaving the origin behind as an unstable equilibrium.

(b) When $\phi \sim 0.3$, $\mathbf{S}_2$ is of the form $(0, e, z)$. Figure 2(b1,2) shows that increasing r_m initially has no influence on the size of both populations e and z. This kind of behaviour gets interrupted once again at $r_m \approx 1.5$ d^{-1}, when stability is transferred from $(0, e, z)$ to $(m, \widetilde{e}, 0)$, $e < \widetilde{e}$. This stability exchange occurs when the two lines shown in Fig. 1(d) coincide, generating a line of nonisolated steady states (shown as vertical lines in panels (b1,2) in Fig. 2).

(c) When $\phi \sim 1$, $\mathbf{S}_2$ is of the form $(m, 0, z)$. The resulting behaviour in this case is identical to what we observed in case (a) (results not shown).

(d) When $k_z/k_e \sim 9$, $\mathbf{S}_2$ is of the form $(m, e, 0)$. The behaviour of the model, in this case, is identical to that of the two-variable model analyzed in (1).

Downloaded from http://journals.aai.org/jimmunol/article-supplement/82846/pdf/jimmunol1001306-sup-suppdata/ by guest on 06 August 2024

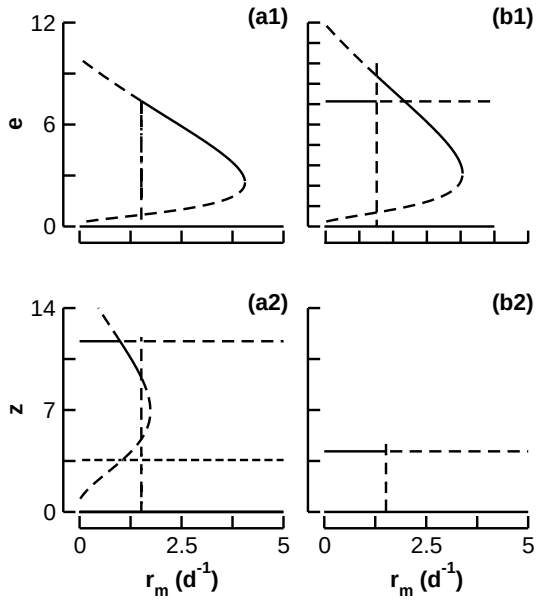

Fig. 2: Bifurcation diagrams of e and z with respect to r_m for high (left) and low (right) levels of relative killing efficacy, ϕ, of the subdominant effector T cells (i.e. of Z relative to E). Stable (unstable) steady states are plotted in solid (dashed) lines. (a) $\phi = 0.8$, (b) $\phi = 0.3$. Panel (b2) shows that treatments aimed at expanding the low-avidity T cell pool may be harmful due to the switch in stability between a steady state with elevated level of high-avidity T cells to another one with even higher level of that population. Vertical lines represent non-isolated steady states.

4 Including thymic input

To examine a variant of the model that includes thymic input, we study Eqs. (6a)-(6c). The bifurcation diagrams of e and z with respect to r_m are plotted in Fig. 3(a) and (b), respectively, for $\phi = 0.8$. We see clearly that the behaviour here is almost identical to that of panels (a1,2) of Fig. 2. By increasing the value of r_m, the subdominant pool, z, gets replaced by the more harmful dominant effector pool, e. Past some threshold, both pools disappear at a saddle node bifurcation (see panel (a) of Fig. 3). The transition from one T cell population to another is expressed by a steep jump similar to case (a) of Fig. 2. This dramatic jump is due to the transition from one steady state close to the mz-plane to another steady state close to the me-plane, as demonstrated in Section 2.1. In other words, we find that thymic input does not alter the qualitative behaviour of the model, other than making the transition from one steady state to another smoother.

5 Modeling treatment

Let $\overline{N}_p$ denote the level of cognate nanoparticles (pMHC-NP) bound to memory cells, N_p denote the level of circulating pMHC-NP, $\widetilde{N}_p$ denote the level of pMHC-NP bound to other T cells and $\widehat{N}_p$ denote the total level of pMHC-NP between two consecutive injections (i.e. $\overline{N}_p + N_p + \widetilde{N}_p = \widehat{N}_p$). We assume that each of these is time

Downloaded from http://journals.aai.org/jimmunol/article-supplement/82846/pdf/jimmunol1001306-sup-suppdata/ by guest on 06 August 2024

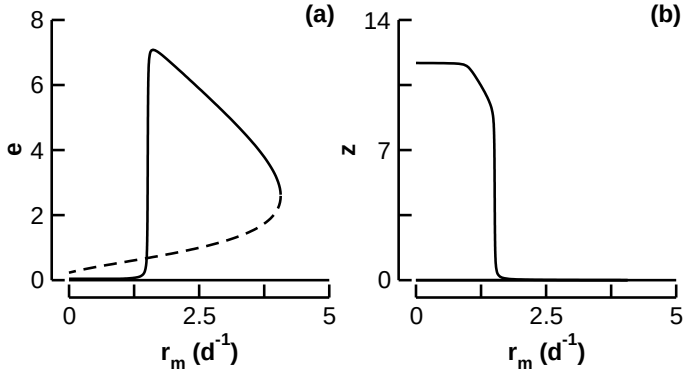

Fig. 3: Bifurcation diagrams of (a) e and (b) z with respect to r_m for $\phi = 0.8$ when the thymic input is included. Stable (unstable) steady states are plotted in solid (dashed) lines. As observed in the previous case, the increase in the size of memory T cell pool may elevate the level of dominant effector T cell pool.

dependent. It follows that $\overline{N}_p$ and N_p satisfy mass-action kinetic equations, given by

$$\frac{d\overline{N}_p}{dt} = k^+ N_p M - k^- \overline{N}_p, \tag{7a}$$

$$\frac{dN_p}{dt} = I(t) + k^- \overline{N}_p - k^+ N_p M - k_u N_p - k_c N_p, \tag{7b}$$

where $I(t)$ is s square wave representing the periodic injections, given by

$$I(t) = \left\{ \begin{array}{ll} d/w & 0 \le t < w \\ 0 & w \le t < T \end{array} \right\}, \quad T > w, \quad I(t+T) = I(t),$$

$k^+ N_p M$ represents the binding of circulating pMHC-NP to memory cells, while $k^- \overline{N}_p$ represents the unbinding of bounded pMHC-NP to memory cells (here multiple binding has been neglected). The terms $k_u N_p$ and $k_c N_p$ represent the loss of pMHC-NP to those unavailable for binding and clearance rates, respectively. If the binding and unbinding of pMHC-NP to memory cells is assumed very rapid, we can apply QSS approximation to Eqn. (7a) and obtain

$$\overline{N}_p \approx \frac{k^+}{k^-} N_p M,$$

which reveals that the rate of expansion of memory cells is proportional to $\overline{N}_p$. Thus

$$\frac{dN_p}{dt} = I(t) - k_u N_p - k_c N_p = I(t) - \delta_{N_p} N_p \quad (\delta_{N_p} = k_u + k_c). \tag{8}$$

6 Treatment protocols

In the biological experiments, NP coated with NRP-V7/K^d or with MimA2/DD^b and complexes were administered by injection to female NOD mice at various doses, ages, and frequencies. In the simulations of our model, we used three treatment protocols that closely mimic the protocols adopted by the Santamaria Lab (2):

Downloaded from http://journals.aai.org/jimmunol/article-supplement/82846/pdf/jimmunol1001306-sup-suppdata/ by guest on 06 August 2024

Protocol 1: (Standard Treatment Protocol) 4 wk-old mice are injected 11 times with a dose d μg (iron) of pMHC-NP (where $d = 7.5$, $7.5/5 = 1.5$ or $7.5/20 = 0.375$ μg). The first three injections are 2 wk apart, and the last 8 injections are 3 wk apart. Measurements of low-avidity memory, high-avidity effector, and subdominant effector clones (M, E, Z) are made 2 wk after the last injection, at 34 wk of age.

Protocol 2: 10 wk-old mice are injected 4 times with $d = 7.5\mu$g of pMHC-NP at the frequency of 2 injections/wk. Measurements of low-avidity memory, high-avidity effector, and subdominant effector clones (M, E, Z) are made at 14 wk of age.

Protocol 3: As in Protocol (2) but with 10 rather than 4 injections and with (M, E, Z) measured at 17 wk of age.

Protocol 4: New onset diabetic mice (blood glucose exceeding 10.5 mM) are injected with $d = 7.5\mu$g pMHC-NP twice-weekly until stably normoglycemic for 4 consecutive wk. Peripheral blood was sampled after the last injection for flow cytometric analysis.

Protocol 5: As in Protocol (4) but with 1 injection per 2-3 wk.

7 Parameter estimation

In order to estimate clonal parameters, we first consider the minimal 3-dimensional model with no thymic input and couple this model to Eqn. (8), governing the dynamics of circulating cognate pMHC-NP. The scaled form of these equations is

$$\frac{dm}{dt} = m\left[\alpha_m f_m(e+\phi z) - \delta_m - \epsilon^*(m+e+z) + r_m^* N_p\right], \tag{9a}$$

$$\frac{de}{dt} = e\left[\alpha_e f_e(e+\phi z) - \delta_e - \epsilon^*(m+e+z) - r_e^* N_p\right], \tag{9b}$$

$$\frac{dz}{dt} = z\left[\alpha_z f_z(e+\phi z) - \delta_z - \epsilon^*(m+e+z)\right], \tag{9c}$$

$$\frac{dN_p}{dt} = I(t) - \delta_{N_p} N_p, \tag{9d}$$

where $r_m \approx r_m^* N_p$, $r_e \approx r_e^* N_p$ and δ_{N_p} is the degradation rate of circulating pMHC-NP.

Detailed kinetic parameters are not available biologically. Values for turnover rates (δ_m, δ_e), rates of proliferation, etc., have been previously estimated in (3, 4). The levels of circulating effector T cells at the height of autoimmunity, together with known turnover rates of effector and memory cells, allowed us in (1) to estimate the rates of proliferation (α_m, α_e) and competition (ϵ). Furthermore, indirect evidence for relative functional avidity of T cell populations allowed us to estimate the ratio k_m/k_e. Based on this fact, it was helpful to consider a substitution $M = k_e m$, $E = k_e e$ and $Z = k_e z$ to obtain a scaled version of the model. The three treatment parameters r_i^*, $i = m, e$, and δ_{N_p}, were estimated using experimental data provided by the Santamaria Lab as described in the paper.

Downloaded from http://journals.aai.org/jimmunol/article-supplement/82846/pdf/jimmunol1001306-sup-suppdata/ by guest on 06 August 2024

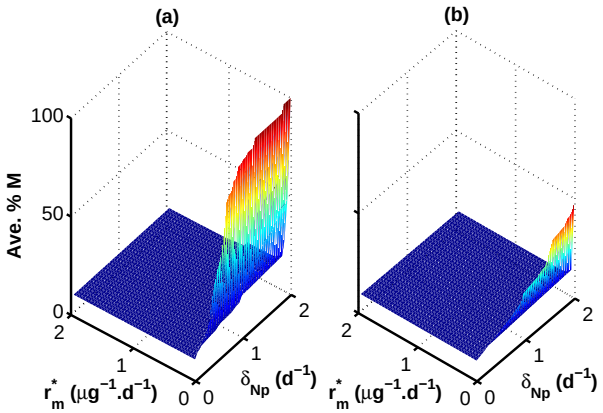

Fig. 4: Average percentage of memory cells in 25 NOD "mice" is calculated for increasing values of δ_{N_p} in the range $0-2$ d^{-1} and r_m^* in the range $0-2$ $(\mu g \cdot d)^{-1}$, (with $r_e^*=0$), after applying Protocol 1 at the two injection doses: (a) $d=1.5$ μg; and (b) $d=0.375$ μg. For each "mouse", all other parameters are selected randomly from uniform distributions within their respective ranges (see Table 1 in the paper). Notice that when r_m^* is set to a fixed small value, the average percentage of memory cells decrease with increasing δ_{N_p}.

Figure 4 shows typically how we estimated the two treatment parameters r_m^* and δ_{N_p} by using Eqs. (9a)-(9d). The average percentage of memory cells in 25 NOD "mice", subjected to the Standard Treatment (Protocol 1), was evaluated for increasing values of δ_{N_p} and r_m^* at two different injections doses; namely, $d=1.5$ μg (panel (a)) and 0.375 μg (panel (b)). The average values that matched the experimental ones very closely (see Fig. 1 of the paper) were selected for further testing using other protocols in order to reduce the size of estimated parameter regime.

8 Including APCs

To examine the effect of hypothesized APC deletion, we consider a heterogeneous population of 500 "mice" with the following model system that ignores thymic input for each one. The full APC model before scaling is

$$\frac{dM}{dt} = M\left[\overline{\alpha}_m A\tilde{f}_m(E+\phi Z)-\delta_m-\frac{\overline{\epsilon}}{A}(M+E+Z)\right], \tag{10a}$$

$$\frac{dE}{dt} = E\left[\overline{\alpha}_e A\tilde{f}_e(E+\phi Z)-\delta_e-\frac{\overline{\epsilon}}{A}(M+E+Z)\right], \tag{10b}$$

$$\frac{dZ}{dt} = Z\left[\overline{\alpha}_z A\tilde{f}_z(E+\phi Z)-\delta_z-\frac{\overline{\epsilon}}{A}(M+E+Z)\right], \tag{10c}$$

$$\frac{dA}{dt} = \sigma_a - k_a MA-\delta_a A. \tag{10d}$$

Downloaded from http://journals.aai.org/jimmunol/article-supplement/82846/pdf/jimmunol1001306-sup-suppdata/ by guest on 06 August 2024

By setting $M = k_e m$, $E = k_e e$, $Z = k_e z$ and $a = A/A_d = A\delta_a/\sigma_a$, and coupling system (10a)-(10d) to Eqn. (8), we obtain the scaled model, given by

$$\frac{dm}{dt} = m\left[\alpha_m^* a f_m(e+\phi z) - \delta_m - \frac{\overline{\epsilon}^*}{a}(m+e+z) + r_m^* N_p\right], \tag{11a}$$

$$\frac{de}{dt} = e\left[\alpha_e^* a f_e(e+\phi z) - \delta_e - \frac{\overline{\epsilon}^*}{a}(m+e+z) - r_e^* N_p\right], \tag{11b}$$

$$\frac{dz}{dt} = z\left[\alpha_z^* a f_z(e+\phi z) - \delta_z - \frac{\overline{\epsilon}^*}{a}(m+e+z)\right], \tag{11c}$$

$$\frac{da}{dt} = \delta(1 - k_a^* m a - a), \tag{11d}$$

$$\frac{dN_p}{dt} = I(t) - \delta_{N_p} N_p, \tag{11e}$$

where $\alpha_i^* = \overline{\alpha}_i \sigma_a/\delta_a$, for $i = m, e$, $\overline{\epsilon}^* = \overline{\epsilon} k_e \delta_a/\sigma_a$ and $k_a^* = k_a k_e/\delta_a$.

We compared the time series of the three pools of T cells for simulated "mice" predicted by this model to those generated by system (9a)-(9d). The recorded responses obtained (results not shown) were almost always identical to the ones observed previously. The competition between the three pools (which implicitly includes the effect of APC-deletion hypothesis) was sufficient to capture all features of system (11a)-(11e).

References

1. Khadra A., P. Santamaria, and L. Edelstein-Keshet. 2009. The role of low avidity T cells in the protection against type 1 diabetes: A modeling investigation. J. Theor. Biol. 256: 126-141.

2. Tsai S., A. Shameli, J. Yamanouchi, X. Clemente-Casares, J. Wang, P. Serra, Y. Yang, Z. Medarova, A. Moore, and P. Santamaria. 2010. Reversal of autoimmunity by boosting memory-like autoregulatory T-cells. Immunity 32: 568-580.

3. Marée A. F. M., P. Santamaria, and L. Edelstein-Keshet. 2006. Modeling competition among autoreactive $CD8^+$ T cells in autoimmune diabetes: implications for antigen-specific therapy. Int. Immunol. 18: 1067-1077.

4. Mahaffy J. M., and L. Edelstein-Keshet. 2007. Modeling cyclic waves of circulating T-cells in autoimmune diabetes. SIAM J. Appl. Math. 67: 915-937.

Downloaded from http://journals.aai.org/jimmunol/article-supplement/82846/pdf/jimmunol1001306-sup-suppdata/ by guest on 06 August 2024